Indones. J. Chem., xxxx, xx (x), xx - xx

1

Strong Anisotropic Rashba Effect with Tunable Spin-Splitting in Two-Dimensional Janus Vanadium Dichalcogenides Monolayer

Yusuf Affandi[1*], Moh. Adhib Ulil Absor[2], Muhammad Anshory[3], and Wardah Amalia[4]

[1]*Instrumentation and Automation Engineering, Faculty of Industrial Technology, Institut Teknologi Sumatera, Way Hui, Lampung Selatan 35365, Indonesia*

[2]*Department of Physics, Faculty of Mathematics and Natural Sciences, Universitas Gadjah Mada, Sekip Utara BLS 21, Yogyakarta 55281, Indonesia*

[3]*Department of Physics, Faculty of Science, Institut Teknologi Sumatera, Way Hui, Lampung Selatan 35365, Indonesia*

[4]*Graduate School of Physics, Department of Physics, Faculty of Mathematics and Natural Sciences, Universitas Gadjah Mada, Sekip Utara BLS 21, Yogyakarta 55281, Indonesia*

Abstract: *Motivated by the recent discovery of the Rashba effect in two-dimensional (2D) Janus Transition Metal Dichalcogenides (TMDs) systems, we explore the Rashba effect on the Janus VXY (X = S, Se, Y = Se, Te) monolayer. By employing first-principles density functional theory (DFT) calculations, we find a strong anisotropic Rashba splitting observed around Γ points in the first Brillouin zone. We analyze this anisotropy of Rashba splitting by using k·p perturbation theory synergized with group symmetry analysis. By giving the effect of the biaxial strain, we manipulate the characteristics of the Rashba splitting on the Janus Vanadium Dichalcogenides system. Through spin texture analysis, we reveal both the in-plane and out-of-plane components of the spin textures, providing further evidence for the anisotropic nature of the Rashba spin-orbit coupling (SOC). The observed tuneable Rashba splitting by applying the strain effect shows that the Janus Vanadium dichalcogenides system has the potential to be used as a semiconductor material for spintronic devices.*

Keywords: *Rashba splitting; density functional theory; strain effect; vanadium dichalcogenides*

■ INTRODUCTION

Spin-orbit interaction (SOI) in low-dimensional material has attracted the attention of researchers over the last decade since it can explain exotic quantum phenomena in solid-state physics. The manipulation of SOI contributes to knowing exciting effects such as the spin Hall effect [1-2], Zeeman effect [3], spin galvanic effect [4-5], and spin ballistic transport [6-7]. Specifically, the Rashba effect has garnered significant attention due to its electrical adjustability, which is the potential for spintronics applications, including the spin-field effect transistor (S-FET).

S-FET are the future transistors that will replace the conventional transistors that have reached their dimensional and performance limits. By utilizing the spin field effect and SOI, S-FET can provide advantages in energy efficiency, operating speed, and high performance of electronic devices [8]. The functionality of the S-FET device is significantly dependent on semiconductor materials with strong Rashba SOI, as indicated by Rashba splitting in the electronic structure around the Fermi level. The Rashba splitting played a vital process called a spin precession, allowing the control of the carrier's spin transport [7] using gate voltage. However, for S-FET devices, the strong Rashba SOI in the semiconductor materials enables working at room temperature.

Some materials with strong Rashba SOI in their electronic structure have been reported due to the

asymmetry of crystal structure [9-11]. Experimental observation of the Rashba SOI is done by angle-resolved photoemission spectroscopy (ARPES) techniques, in the case of BiInAs [12], PtBi$_2$ [13] and CH$_3$NH$_3$PbBr$_3$ organic-inorganic perovskite [14], and magnetotransport measurements, like in the case of Fe/Ge(111) [15]. Theoretical investigation has predicted that Rasbha splitting exists in many 2D materials such as polar perovskite [16], black-phosphorene [17], BiTeI [18], Janus structure of group IV-V materials [10,19], transition metal dichalcogenides (TMDs) [20], and Janus transition metal dichalcogenides [9,11,21-22].

TMDs have the formula MX$_2$ where M represents transition metal atoms and X corresponds to chalcogen atoms such as sulfur (S), selenium (Se), and tellurium (Te). On the other hand, Janus TMDs are derived from the original TMDs monolayer (ML) with the formula MXY, where one of the X chalcogen atoms is replaced by a different chalcogen atom denoted as Y. This substitution introduces asymmetry into the structure, leading to a non-uniform charge distribution. Consequently, the symmetry breaking in Janus TMDs results in Rashba SOI-induced spin splitting at the Brillouin zone, particularly noticeable at the valence band maximum (VBM).

Recent advancements in material synthesis have successfully produced Janus TMDs, such as MoSSe ML fabricated through the selenization of MoS$_2$ [23] and a sulfurization process from MoSe$_2$ [24], as well as the WSSe thin film by chemical vapor deposition [25]. These experimental achievements have spurred theoretical investigations into the family of Janus TMDs. However, considerable interest remains in exploring additional 2D material systems that exhibit Rashba splitting due to its potential significance in spintronics applications.

The discovery of new materials with Rashba splitting not only enriches our understanding of spin-dependent phenomena but also broadens the scope of materials available for applications in spintronics, offering opportunities for developing novel electronic and optoelectronic devices. Therefore, ongoing efforts to identify and characterize such materials are highly valued in both theoretical and experimental research communities. The successful computational investigation

of heterostructure TMDCs has also confirmed the generation of significant Rashba spin-splitting, suggesting TMDCs as promising candidates for spintronics applications [26-27]. In the realm of heterostructure applications, the significance of strain effects is highlighted, particularly within the fabrication process, where misfit dislocations occur when creating materials with distinct lattice parameters compared to the substrate [28].

Among the Janus TMDs, studies regarding VXY (X, Y = S, Se, Te) have been gaining some attention, mainly focusing on structural stability, electronic, and magnetic properties [29-31]. While VXY MLs have not been synthesized, the successful synthesis of the Janus Transition Metal Dichalcogenides [23] suggests the potential realization of VXY MLs. Therefore, to complement previous research, in this paper, we predict and discuss the emergence of anisotropic Rashba splitting in the two-dimensional (2D) Janus Vanadium Dichalcogenides VXY (X, Y = S, Se, Te) using first-principles density functional theory (DFT) calculation and the $\vec{k} \cdot \vec{p}$ perturbation theory analysis. In our study, the electronic structure properties of VXY ML exhibit a semiconducting with an indirect band gap. Moreover, we observe the emergence of anisotropic Rashba splitting around Γ point in VBM, similar to other Janus TMDs. In our analysis of Rashba splitting using $\vec{k} \cdot \vec{p}$ perturbation theory, we found the strong Rashba SOI of the VSeTe with the Rashba parameter of 0.12 eVÅ. Additionally, our study highlights that both the bandgap and Rashba splitting can be controlled by biaxial strain. These findings hold promise for future applications in spintronics, underscoring the significance of continued research efforts in this field.

■ EXPERIMENTAL SECTION

This work employs the DFT calculations utilizing Generalized Gradient Approximation (GGA) [32], as implemented in OpenMX code [33]. Norm-conserving pseudopotentials with an energy cutoff of 250 Ry for charge density were utilized to ensure accurate representations of electronic structures and interactions within the system. By utilizing a confinement scheme

[34-35], we employed the linear combination of multiple pseudoatomic orbitals to expand the wavefunction, where two s-, two p-, and one d- character numerical pseudo-atomic orbitals were used for each atom. The SOI was included in our calculation by j-dependent pseudopotentials [36]. These computational methods enable thorough investigations into the properties and behaviors of the materials under study, offering insights into their structural, electronic, and energetic characteristics.

The primary focus of our computational calculations revolves around the Janus vanadium dichalcogenides VXY monolayer system, comprising VSSe, VSTe, and VSeTe. We construct the crystal structure of Janus vanadium dichalcogenides by a trigonal prismatic known as the type 2H polymorph, which manifests as the most stable structure of TMDs under room temperature. Fig. 1(a) and 1(c) present detailed depictions of the Janus VXY monolayer from both top and side perspectives, elucidating its structural intricacies. In this configuration, a single transition metal atom V forms bonds with two distinct chalcogen atoms, resulting in a polar system characterized by varying V−X and V−Y

distances. This non-centrosymmetric structure aligns with the C_{3v} point group symmetry. Such structural details lay the groundwork for further analysis, particularly within the framework of k·p perturbation theory, allowing us to delve deeper into the electronic properties and behaviors of these intriguing materials.

In our computations, we represent the two-dimensional structures of VXY ML by constructing a periodic slab with a sufficiently large vacuum layer of 24 Å to eliminate any interactions between adjacent layers effectively. To accurately capture the electronic properties, an $8 \times 8 \times 1$ k-point mesh is utilized, ensuring thorough coverage of the Brillouin zone. Furthermore, atomic positions undergo complete relaxation, adhering to a 1×10^{-5} Hartree/Bohr force criterion to achieve stable geometries. The first Brillouin zone of this material system exhibits distinct high symmetry points, including M, K, Q, and Γ as shown in Fig. 1(b). Then we consider the biaxial strain effect with a range from −5% to 5% to know the changes of band structure, especially Rashba splitting due to this effect. Notably, electronic structure calculations are conducted post-full relaxation of all atoms under each strain condition, ensuring an
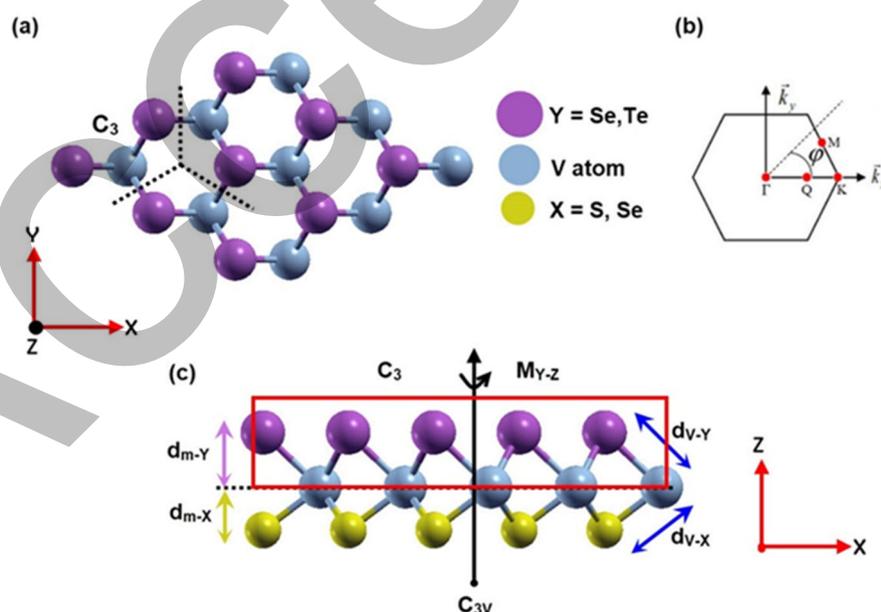

Fig 1. Illustrations of the Janus VXY monolayer from both (a) top and (c) side perspectives, with atomic distances along the z-axis denoted as $d_{m−Y}$ and $d_{m−X}$, bond lengths indicated as $d_{V−X}$ and $d_{V−Y}$, along with the symmetry group of the Janus VXY monolayer. (b) The first Brillouin zone in the k space is shown, highlighting high symmetry points (Γ, M, K)

accurate depiction of the system's response to mechanical deformation.

■ RESULTS AND DISCUSSION

First, we discuss the structural symmetry of VXY MLs. We have obtained the optimized structural parameters shown in Table 1. The optimized lattice constants a_0 are 3.210 (VSSe ML), 3.432 (VSTe ML) and 3.450 Å (VSeTe ML), which are consistent with previous work [29-30]. It has been observed that the lattice constant of VXY MLs increases as the atomic number of chalcogen atoms XY increases. In addition, we also get the bond length of V–X(Y) $d_{V–X}$($d_{V–Y}$) as shown in Table 1. The difference between $d_{V–X}$ and $d_{V–Y}$ for each monolayer system indicated that these systems are non-centrosymmetry crystal structures However, its structural parameters ($d_{V–X}$ and $d_{V–Y}$), also increase as the atomic

number of chalcogen atoms (X and Y) increases.

Next, we calculated the electronic structure of VSSe, VSTe, and VSeTe ML with results in Fig. 2 VSSe ML (Fig. 1(a)) and VSeTe (Fig. 1(c)) shows the semiconducting properties with bandgap energy are 0.86 and 0.57 eV, respectively. The natural differences are evident in the VSTe ML (Fig. 1(b)), where the electronic structure displays metallic properties with zero energy gap. As a representative, we calculated the projected orbital band of the VSeTe ML shown in Fig. 2. It is clear that the valence band maximum (VBM) is characterized by two local maxima positioned at the K and Γ points. At the K point, the occupied state predominantly arises from the coupling of in-plane atomic orbitals, namely $d_{x^2} - d_{y^2} + d_{xy}$. Conversely, the occupied state at the Γ point is attributed to contributions from both out-of-plane atomic orbitals $d_{3z^2-r^2}$ and p_z,

Table 1. The optimized structural parameters of VXY monolayer systems, including Lattice constant a, V-chalcogen bonding lengths $d_{V–X}$ and $d_{V–Y}$, and the distance between two chalcogen atoms ($d_{X–Y}$)

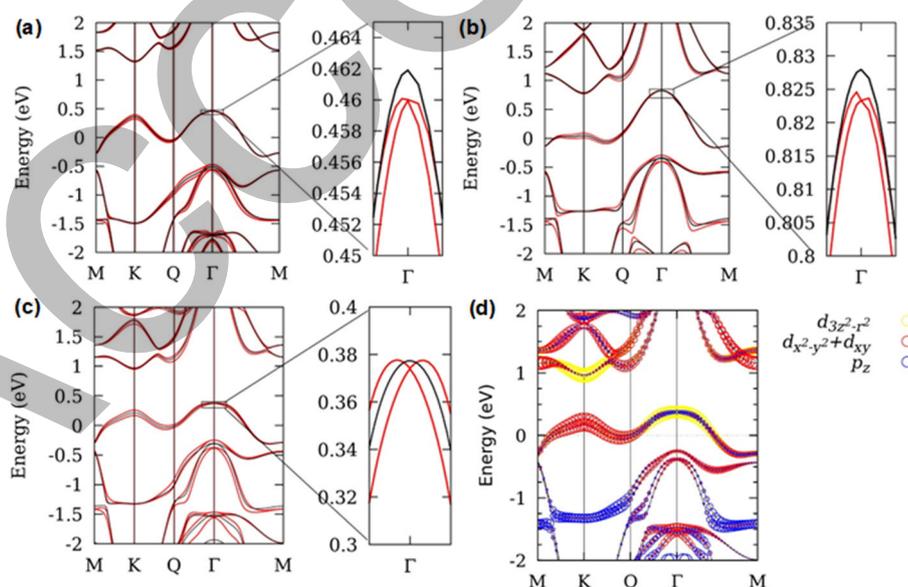| No	VXY monolayer system	a (Å)	$d_{V–X}$ (Å)	$d_{V–Y}$ (Å)	$d_{m–X}$ (Å)	$d_{m–Y}$ (Å)	E_{gap} (eV)
1	VSSe	3.210	2.36	2.51	1.73	1.93	0.86
2	VSTe	3.432	2.37	2.79	1.64	2.20	0.00
3	VSeTe	3.450	2.50	2.77	1.81	2.17	0.57

Fig 2. The electronic band structure of (a) VSSe, (b) VSTe, and (c) VSeTe monolayers with and without SOI indicated by red and black lines, respectively, focusing on magnifications around Γ point. Panel (d) illustrates the projected orbital band of the VSeTe monolayer, with colored orbital contributions, and the spectral weights depicted by circle radii

which are also responsible for the emergence of Rashba splitting that appears at the point. In contrast to VBM, the conduction band minimum (CBM) is situated at the K point, primarily contributed by the $d_{3z^2-r^2}$ atomic orbital.

Incorporating SOI into the electronic structure calculation, as denoted by the red line, reveals notable Zeeman splitting around the K point in VBM for all systems VSSe ML, VSTe ML, and VSeTe ML systems, attributable to the breaking of time-reversal symmetry (Fig. 1(a)-(c)). However, our primary focus lies on another form of splitting known as Rashba splitting, which is also evident in the electronic structure of all systems, particularly noticeable in the VBM around Γ point. In the VSeTe ML system, this Rashba splitting is pronounced due to the substantial SOI originating from both Se and Te atoms, coupled with the broken inversion symmetry within the system. Conversely, in VSSe ML and VSTe ML, the SOI contributions solely from Se and Te atoms result in weaker Rashba splitting compared to VSeTe ML. Notably, similar Rashba splitting phenomena are observed in all Janus Mo and W dichalcogenides [9,37]. This highlights the importance of considering SOI effects in understanding the electronic properties of these materials, particularly their potential applications in spintronics and related fields.

Moving forward, we delve into the examination of the biaxial strain effect (compressive and expansive strain) on the electronic structure of VSeTe ML, with a range from −5% to 5%. This effect can be experimentally expected by introducing the substrates during the growth process of the monolayer [23-24]. In this case, we use the ideal range of strain effect (−5% to 5%) to ensure that the system does not undergo deformation. Moreover, this range is well-suited for experimental implementation using the substrate-induced strain method [38-39]. We defined the degree of biaxial strain as Eq. (1).

$$\varepsilon_i = \frac{(a_i - a_0)}{a_0}100\% \qquad (1)$$

where a_i and a_0 are the lattice constant of strained and equilibrium structures. Fig. 3 shows the evolution of the band structure of VSeTe ML with respect to the biaxial strain effect. Due to the compressive strain effect the VBM swift from K point to Γ point. The same thing was also observed in the CBM which swiftly from K point to the midpoint between K and Γ points, which we call the Q point. Consequently, the indirect band gap remains, but the optical transition changes dramatically from the K(CBM) – Γ(VBM), to the Q(CBM) – K(VBM). Meanwhile, no shifting occurs between CBM and VBM under the expansive strains effect, but it was observed that the energy gap decreases as the degree of expansive strains increases, and it is predicted to reach metallic properties for a high degree of expansive strain.

In other words, strain application also influences Janus VXY ML's electronic properties. The application of compressive strain up to −5% results in an increased energy band gap of these materials. Conversely, applying expansive strain up to 5% leads to a decrease in the energy band gap of this material, allowing a transition from semiconductor properties to metallic properties for a high degree of expansive strain.
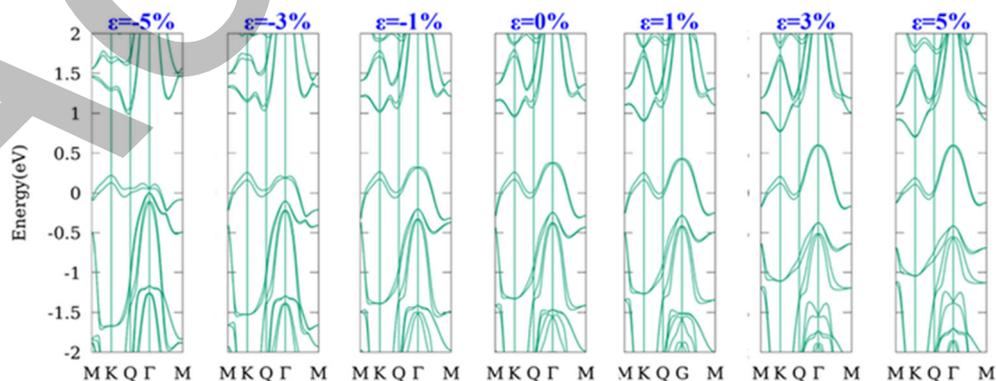

Fig 3. The variation in strain (compressive and expansive strain) induces changes in the electronic structure of the VSeTe monolayer

The substantial evolution of the electronic structures of the VSeTe ML by biaxial strain effect is expected to induce a significant change of the Intrinsic Rashba splitting band around Γ point. Essentially, this intrinsic Rashba effect is inherent in Janus VXY systems due to the presence of an out-of-plane potential gradient, resulting from the crystal's non-centrosymmetry (lacking the inversion symmetry), which is absent in non-Janus systems. The application of the biaxial strain effect makes it possible to control the out-of-plane potential gradient, as indicated by the change in magnitude of d_{m-X} and d_{m-Y} (see Fig. 1(c)). Therefore, the imposition of biaxial strain results in structural alterations in the VXY MLs material, indicated by changes in d_{m-X} and d_{m-Y}. Consequently, it can be stated that the application of biaxial strain allows for the control and manipulation of Rashba splitting in the VXY MLs. This is achieved by modifying its structure without altering its crystal structure, which remains preserved within the C_{3v} symmetry group.

We use perturbation theory based on the symmetry group to further analyze the origin Rashba splitting in the Janus VXY MLs systems. The Rashba Hamiltonian is derived by evaluating the irreducible representation of the system within its designated symmetry group. The Janus VXY MLs has a crystal symmetry of C_{3v} point group. In systems possessing C_{3v} symmetry, the effective Hamiltonian at around the Γ point can be articulated as Eq. (2) [9,20,37,40];

$$H(R) = E_0(k) + \alpha(k)[\cos(\phi)\sigma_y - \sin(\phi)\sigma_x] + \alpha_3^2 k^3 \cos(3\phi)\sigma_z \quad (2)$$

where $E_0(k) = \frac{k^2}{2m*}$, $m*$ is effective mass, $\alpha(k) = \alpha_1 k + \alpha_3^1$, with α_1 and α_3^1 are the first and third order Rashba parameters, respectively, while α_3^2 is the warping parameter. Furthermore, we introduce a polar angle ϕ in k space, defined as $\phi = \cos^{-1}(\frac{k_x}{k})$, where the k_x is chosen to be parallel with the Γ – K line in the first Brillouin zone

(refer to Fig. 1(b)). By solving the eigenvalue problem associated with the Hamiltonian, we derive the spin-splitting energy expressed in square form as expressed in Eq. (3).

$$[\Delta\varepsilon(k)]^2 = (\alpha_1 k + \alpha_3^1 k^3)^2 + (\alpha_3^2)^2 k^6 \cos^2(3\phi) \quad (3)$$

The Rashba parameter of VXY MLs results from fitting calculations using Eq. 3 for small k, as shown in Table 2 and Fig. 4(a). The values of α_1 calculated for Γ – M direction are 0.03, 0.05, and 0.12 eVÅ, while for Γ – K direction are 0.03, 0.05, and 0.12 eVÅ for VSSe, VSTe, and VSeTe ML, respectively. These results reinforce that the VSeTe ML has a stronger Rashba SOI than VSSe and VSTe ML, attributed to the strong SOI contributed by Se and Te atoms. Moreover, it is evident that the Rashba splitting is anisotropic for all equilibrium systems. This result is slightly different from the findings of previous research [29], which obtained Rashba parameter values of 0 eVÅ for VSSe, VSTe MLs, and 0.685 eVÅ for VSeTe ML. However, our study provides more comprehensive results, in which the Rashba parameter values are also contributed by the third-order part, indicating anisotropic Rashba splitting. Our results also exhibit slightly smaller Rashba parameter values compared to findings in other studies on WSeTe material [41]. This is likely due to Tungsten exerting a larger SOI influence than Vanadium. Furthermore, a prior study [41] explored the impact of Pb adsorption on Rashba splitting in WSeTe. Our research will investigate the influence of strain effects on the electronic structure and Rashba splitting of VXY monolayers.

Subsequently, we explore the impact of strain on Rashba splitting in Janus VXY monolayers. We use VSeTe ML as a representative due to the strongest intrinsic Rashba splitting when applying the strain effect.

Table 2. Rashba Parameter fitting results in VXY Monolayers equilibrium systems including the first, and third-order parameters

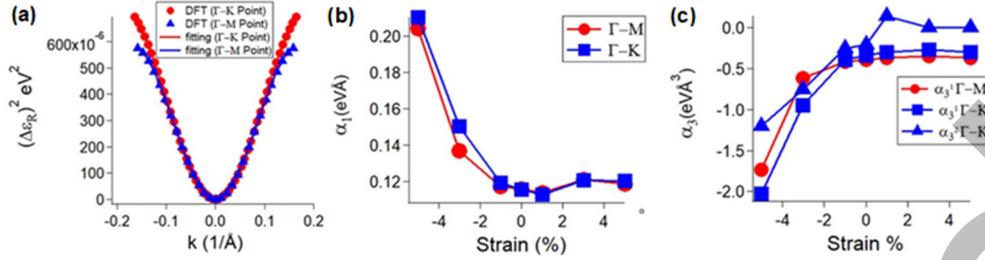| Systems	Γ – M		Γ – K		
	α_1 (eVÅ)	α_3^1 (eV Å³)	α_1 (eVÅ)	α_3^1 (eV Å³)	α_3^2 (eVÅ³)
VSSe ML	0.03	-0.16	0.03	-0.15	0.13
VSTe ML	0.05	-0.06	0.05	-0.04	0.14
VSeTe ML	0.12	-0.39	0.12	-0.34	-0.20

Fig 4. (a) The square energy Rashba splitting $[\Delta\varepsilon(k)]^2$ for the VSeTe monolayer in equilibrium calculated along $\Gamma - K$ (blue) and $\Gamma - M$ (red) direction in comparison to the fitting results, the strain percentage of the Janus VSeTe Monolayer is depicted as a function of (b) the first-order Rashba parameter in $\Gamma - K$ and $\Gamma - M$ direction, (c) the third-order Rashba parameter in $\Gamma - K$ and $\Gamma - M$ direction

It is evident from our observations that the application of strain markedly influences the difference in distance, denoted as Δz ($\Delta z = |d_{m-X} - d_{m-Y}|$) between Se and Te atoms. Consequently, there is a change in the Rashba splitting energy of the strained VSeTe system. In Fig. 4(b), it can be seen that the first-order Rashba parameter α_1 follows a similar trend in both $\Gamma - M$ and $\Gamma - K$ directions, showing a notable increase with an increase in compressive strain. Under 5% compressive strain, the α_1 value of the VSeTe ML extends to 0.21 eVÅ. This result yields a larger value compared to semiconductor heterostructures such as InGaAs/InAlAs (0.07 eVÅ) [42], the oxide interface LaAlO₃/SrTiO₃ (0.01–0.05 eVÅ) [43] and is comparable to the Janus MoSSe [9] and Tungsten Dichalcogenides influenced by external electric field [20]. Moreover, with an increase in compressive strain, there is a noticeable rise in the α_1 disparity between the $\Gamma - M$ and $\Gamma - K$ directions. This signifies a shift in the Rashba splitting properties from being isotropic at the equilibrium state to becoming anisotropic in the system

under the compressive strain. This observation is further supported by the outcomes of the third-order Rashba parameters α_3^1 and α_3^2 in both directions. These parameters exhibit a negative increase under compressive strain, as depicted in Fig. 4(c).

To further confirm the presence of Rashba splitting in Janus VSeTe ML, the spin-resolved constant energy 2D spin textures are additionally depicted in Fig. 5. We compared the spin textures around the Γ point in equilibrium system Fig. 5(b) with those in the strained system, under compressive (Fig. 5(a)) and expansive (Fig. 5(c)) strain of VSeTe ML. In both systems, it has been verified that the emergence of Rashba spin splitting around the Γ point for small k values comprises two spin components, manifesting in clockwise and counterclockwise directions. The equilibrium system exhibits an imperfectly circular spin texture shape (slightly showing hexagonal shape) indicating anisotropic Rashba splitting. The compressed system displays a more pronounced hexagonal spin texture, indicating the
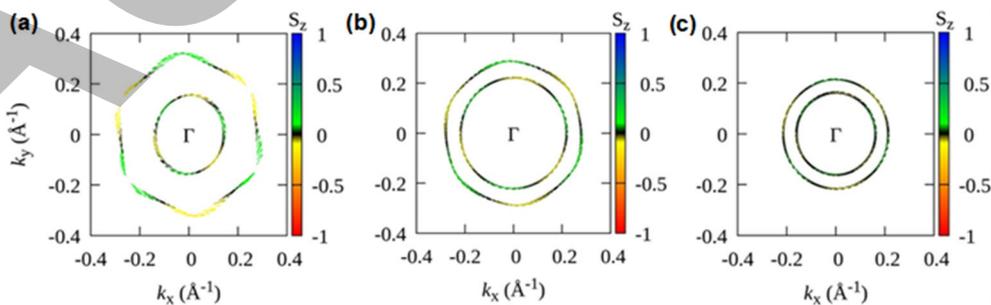

Fig 5. The Spin Texture of the Janus VSeTe monolayer around Γ point with (a) compressive strain of 3%, in equilibrium (b), and with (c) expansive strain of 3%, indicates the evolution of Rashba splitting due to the strain effect. The arrows in the figure symbolize the directions of spin, while the color scale illustrates the out-of-plane components of spin

strong anisotropic Rashba splitting. On the contrary, the expansive strain transforms the Rashba, splitting it into an isotropic form. This can be explained by the absolute value of the third-order Rashba parameters (α_3^1 and α_3^2), which increases as the compressive strain increases and gets closer to zero as the expansive strain increases.

Our research outcomes mark a significant stride in unraveling the complexities of Rashba splitting in two-dimensional (2D) materials. Beyond the triumph in crafting the Janus Transition Metal Dichalcogenides ML [23-24,44-46], our projections extend ambitiously to the foreseen synthesis of VXY MLs. Our research provides additional references as candidate materials for S-FET devices. However, our results also indicate that the strength of Rashba splitting in VXY ML materials is solely attributed to the strong SOI of Se and Te atoms. In addition to the applied strain effects we have conducted, there's potential to augment the magnitude of spin splitting in these materials by introducing heavier elements with strong SOI through doping [47]. This approach makes this phenomenon's experimental detection more attainable, especially through methodologies like spin-resolved photoemission spectroscopy. This foresight opens vistas for VXY MLs to evolve into pivotal 2D semiconductors, poised to revolutionize the landscape of spintronic applications, notably in the realm of S-FETs.

■ CONCLUSION

We have investigated the intriguing Rashba splitting phenomenon in two-dimensional Janus Vanadium Dichalcogenides through extensive first-principles DFT calculations. Our study reveals a substantial intrinsic Rashba splitting concentrated around the Γ point within the VBM. By analyzing the symmetry group and employing the k · p theory, we have validated that the anisotropic characteristics of Rashba splitting stem from the third-order term within the effective Hamiltonian. Notably, we observed that the Rashba splitting can be effectively controlled and modulated by the application of strain with the ideal ranges, highlighting the potential for precise control over this phenomenon. Our results provide a fundamental understanding of the Rashba effect

in 2D Janus TMDs, revealing interesting functionalities that can potentially be applied in spintronics. These insights provide a groundwork for experimental exploration, opening up possibilities for further investigations into the practical utilization of these materials.

■ CONFLICT OF INTEREST

The authors have declared that no competing interest exist.

■ AUTHOR CONTRIBUTIONS

Yusuf Affandi conducted the DFT calculations and wrote the manuscript. Muhammad Anshory and Wardah Amalia conducted the DFT calculations. Moh. Adhib Ulil Absor provided the conceptualization and correction the manuscript. All authors agreed to the final version of this manuscript.

■ REFERENCES

[1] Sinova, J., Valenzuela, S.O., Wunderlich, J., Back, C.H., and Jungwirth, T., 2015, Spin hall effects, *Rev. Mod. Phys.*, 87 (4), 1213–1260.

[2] Bandurin, D.A., Tyurnina, A.V., Yu, G.L., Mishchenko, A., Zólyomi, V., Morozov, S.V., Kumar, R.K., Gorbachev, R.V., Kudrynskyi, Z.R., Pezzini, S., Kovalyuk, Z.D., Zeitler, U., Novoselov, K.S., Patenè, A., Eaves, L., Grigorieva, I.V., Fal'ko, V.I., Geim, A.K., and Cao, Y., 2017, High electron mobility, quantum Hall effect and anomalous optical response in atomically thin InSe, *Nat. Nanotechnol.*, 12 (3), 223–227.

[3] Wang, T., Miao, S., Li, Z., Meng, Y., Lu, Z., Lian, Z., Blei, M., Taniguchi, T., Watanabe, K., Tongay, S., Smirnov, D., and Shi, S.F., 2020, Giant valley-zeeman splitting from spin-singlet and spin-triplet interlayer excitons in WSe_2/$MoSe_2$ heterostructure, *Nano Lett.*, 20 (1), 694–700.

[4] Seibold, G., Caprara, S., Grilli, M., and Raimondi, R., 2017, Theory of the spin galvanic effect at oxide interfaces, *Phys. Rev. Lett.*, 119 (25), 256801.

[5] Benítez, L.A., Savero Torres, W., Sierra, J.F., Timmermans, M., Garcia, J.H., Roche, S., Costache, M.V., and Valenzuela, S.O., 2020, Tunable room-temperature spin galvanic and spin Hall effects in van der Waals heterostructures, *Nat. Mater.*, 19 (2), 170–175.

[6] Borge, J., and Tokatly, I.V., 2017, Ballistic spin transport in the presence of interfaces with strong spin-orbit coupling, *Phys. Rev. B*, 96 (11), 115445.

[7] Rao, Q., Kang, W.H., Xue, H., Ye, Z., Feng, X., Watanabe, K., Taniguchi, T., Wang, N., Liu, M.H., and Ki, D.K., 2023, Ballistic transport spectroscopy of spin-orbit-coupled bands in monolayer graphene on WSe_2, *Nat. Commun.*, 14 (1), 6124.

[8] Datta, S., and Das, B., 1990, Electronic analog of the electro-optic modulator, *Appl. Phys. Lett.*, 56 (7), 665–667.

[9] Putri, S.A., Suharyadi, E., and Absor, M.A.U., 2021, Polarity effect on the electronic structure of molybdenum dichalcogenides moxy (X, Y = S, Se): A computational study based on density-functional theory, *Indones. J. Chem.*, 21 (3), 598–608.

[10] Lukmantoro, A., and Absor, M.A.U., 2023, Anisotropic Rashba splitting dominated by out-of-plane spin polarization in two-dimensional Janus XA_2Y (A = Si, Sn, Ge; X, Y = Sb, Bi) with surface imperfection, *Phys. Rev. Mater.*, 7 (10), 104005.

[11] Sino, P.A.L., Feng, L.Y., Villaos, R.A.B., Cruzado, H.N., Huang, Z.Q., Hsu, C.H., and Chuang, F.C., 2021, Anisotropic Rashba splitting in Pt-based janus monolayers PtXY (X,Y = S, Se, or Te), *Nanoscale Adv.*, 3 (23), 6608–6616.

[12] Nakamura, T., Ohtsubo, Y., Yamashita, Y., Ideta, S., Tanaka, K., Yaji, K., Harasawa, A., Shin, S., Komori, F., Yukawa, R., Horiba, K., Kumigashira, H., and Kimura, S., 2018, Giant Rashba splitting of quasi-one-dimensional surface states on Bi/InAs(110)-(2 × 1), *Phys. Rev. B*, 98 (7), 075431.

[13] Feng, Y., Jiang, Q., Feng, B., Yang, M., Xu, T., Liu, W., Yang, X., Arita, M., Schwier, E.F., Shimada, K., Jeschke, H.O., Thomale, R., Shi, Y., Wu, X., Xiao, S., Qiao, S., and He, S., 2019, Rashba-like spin splitting along three momentum directions in trigonal layered $PtBi_2$, *Nat. Commun.*, 10 (1), 4765.

[14] Niesner, D., Wilhelm, M., Levchuk, I., Osvet, A., Shrestha, S., Batentschuk, M., Brabec, C., and Fauster, T., 2016, Giant Rashba splitting in $CH_3NH_3PbBr_3$ organic-inorganic perovskite, *Phys. Rev. Lett.*, 117 (12), 126401.

[15] Guillet, T., Marty, A., Vergnaud, C., Jamet, M., Zucchetti, C., Isella, G., Barbedienne, Q., Jaffrès, H., Reyren, N., George, J.M., and Fert, A., 2021, Large Rashba unidirectional magnetoresistance in the Fe/Ge(111) interface states, *Phys. Rev. B*, 103 (6), 064411.

[16] Chen, J., Wu, K., Hu, W., and Yang, J., 2021, Tunable Rashba spin splitting in two-dimensional polar perovskites, *J. Phys. Chem. Lett.*, 12 (7), 1932–1939.

[17] Popović, Z.S., Kurdestany, J.M., and Satpathy, S., 2015, Electronic structure and anisotropic Rashba spin-orbit coupling in monolayer black phosphorus, *Phys. Rev. B*, 92 (3), 035135.

[18] Zhang, S.H., and Liu, B.G., 2019, Anisotropic Rashba effect and charge and spin currents in monolayer BiTeI by controlling symmetry, *Phys. Rev. B*, 100 (16), 165429.

[19] Affandi, Y., Darojat, Y., Anshory, M., and Masfufah, A., 2024, Computational exploration of intrinsic Rashba splitting in Janus Si_2SbBi monolayer using density functional theory, *J. Energy, Mater. Instrum. Technol.*, 5 (1), 28–34.

[20] Affandi, Y., and Ulil Absor, M.A., 2019, Electric field-induced anisotropic Rashba splitting in two dimensional tungsten dichalcogenides WX_2 (X: S, Se, Te): A first-principles study, *Phys. E*, 114, 113611.

[21] Chen, J., Wu, K., Ma, H., Hu, W., and Yang, J., 2020, Tunable Rashba spin splitting in Janus transition-metal dichalcogenide monolayers *via* charge doping, *RSC Adv.*, 10 (11), 6388–6394.

[22] Anshory, M., Darojat, Y., and Affandi, Y., 2024, Electric field controlled anisotropic Rashba

splitting in Janus chromium dichalcogenide monolayers: A computational study based on density functional theory, *JTAF*, 12 (1), 49–56.

[23] Lu, A.Y., Zhu, H., Xiao, J., Chuu, C.P., Han, Y., Chiu, M.H., Cheng, C.C., Yang, C.W., Wei, K.H., Yang, Y., Wang, Y., Sokaras, D., Nordlund, D., Yang, P., Muller, D.A., Chou, M.Y., Zhang, X., and Li, L.J., 2017, Janus monolayers of transition metal dichalcogenides, *Nat. Nanotechnol.*, 12 (8), 744–749.

[24] Zhang, J., Jia, S., Kholmanov, I., Dong, L., Er, D., Chen, W., Guo, H., Jin, Z., Shenoy, V.B., Shi, L., and Lou, J., 2017, Janus monolayer transition-metal dichalcogenides, *ACS Nano*, 11 (8), 8192–8198.

[25] Trivedi, D.B., Turgut, G., Qin, Y., Sayyad, M.Y., Hajra, D., Howell, M., Liu, L., Yang, S., Patoary, N.H., Li, H., Petrić, M.M., Meyer, M., Kremser, M., Barbone, M., Soavi, G., Stier, A.V., Müller, K., Yang, S., Esqueda, I.S., Zhuang, H., Finley, J.J., and Tongay, S., 2020, Room-temperature synthesis of 2D Janus crystals and their heterostructures, *Adv. Mater.*, 32 (50), 2006320.

[26] Xiang, L., Ke, Y., and Zhang, Q., 2019, Tunable giant Rashba-type spin splitting in PtSe$_2$/MoSe$_2$ heterostructure, *Appl. Phys. Lett.*, 115 (20), 203501.

[27] Din, H.U., Idrees, M., Albar, A., Shafiq, M., Ahmad, I., Nguyen, C.V., and Amin, B., 2019, Rashba spin splitting and photocatalytic properties of GeC-MSSe (M = Mo, W) van der Waals heterostructures, *Phys. Rev. B*, 100 (16), 165425.

[28] Gabrys, P.A., Seo, S.E., Wang, M.X., Oh, E., Macfarlane, R.J., and Mirkin, C.A., 2018, Lattice mismatch in crystalline nanoparticle thin films, *Nano Lett.*, 18 (1), 579–585.

[29] Lv, M.H., Li, C.M., and Sun, W.F., 2022, Spin-orbit coupling and spin-polarized electronic structures of Janus vanadium-dichalcogenide monolayers: First-principles calculations, *Nanomaterials*, 12 (3), 382.

[30] Dey, D., and Botana, A.S., 2020, Structural, electronic, and magnetic properties of vanadium-based Janus dichalcogenide monolayers: A first-principles study, *Phys. Rev. Mater.*, 4 (7), 74002.

[31] Zhang, C., Nie, Y., Sanvito, S., and Du, A., 2019, First-principles prediction of a room-temperature ferromagnetic Janus VSSe monolayer with piezoelectricity, ferroelasticity, and large valley polarization, *Nano Lett.*, 19 (2), 1366–1370.

[32] Perdew, J.P., Burke, K., and Ernzerhof, M., 1996, Generalized gradient approximation made simple, *Phys. Rev. Lett.*, 77 (18), 3865–3868.

[33] Ozaki, T., Kino, H., Yu, J., Han, M.J., Kobayashi, N., Ohfuti, M., Ishii, F., Ohwaki, T., Weng, H., and Terakura, K., 2009, *OpenMX: Open source package for Material eXplorer*, http://www.openmx-square.org/.

[34] Ozaki, T., 2003, Variationally optimized atomic orbitals for large-scale electronic structures, *Phys. Rev. B*, 67 (15), 155108.

[35] Ozaki, T., and Kino, H., 2004, Numerical atomic basis orbitals from H to Kr, *Phys. Rev. B*, 69 (19), 195113.

[36] Theurich, G., and Hill, N.A., 2001, Self-consistent treatment of spin-orbit coupling in solids using relativistic fully separable *ab initio* pseudopotentials, *Phys. Rev. B*, 64 (7), 073106.

[37] Absor, M.A.U., Santoso, I., Harsojo, H., Abraha, K., Kotaka, H., Ishii, F., and Saito, M., 2017, Polarity tuning of spin-orbit-induced spin splitting in two-dimensional transition metal dichalcogenides, *J. Appl. Phys.*, 122 (15), 153905.

[38] Chae, W.H., Cain, J.D., Hanson, E.D., Murthy, A.A., and Dravid, V.P., 2017, Substrate-induced strain and charge doping in CVD-grown monolayer MoS$_2$, *Appl. Phys. Lett.*, 111 (14), 143106.

[39] Kumar, S., Kaczmarczyk, A., and Gerardot, B.D., 2015, Strain-induced spatial and spectral isolation of quantum emitters in mono- and bi-layer WSe$_2$, *Nano Lett.*, 15 (11), 7567–7573.

[40] Vajna, S., Simon, E., Szilva, A., Palotas, K., Ujfalussy, B., and Szunyogh, L., 2012, Higher-order contributions to the Rashba-Bychkov effect with application to the Bi/Ag(111) surface alloy, *Phys. Rev. B*, 85 (7), 075404.

[41] Yang, C., Li, J., Liu, X., and Bai, C., 2023, The tunable anisotropic Rashba spin–orbit coupling effect in Pb-adsorbed Janus monolayer WSeTe, *Phys. Chem. Chem. Phys.*, 25 (42), 28796–28806.

Indones. J. Chem., xxxx, xx (x), xx - xx

11

[42] Nitta, J., Akazaki, T., Takayanagi, H., and Enoki, T., 1997, Gate control of spin-orbit interaction in an inverted $In_{0.53}Ga_{0.47}As/In_{0.52}Al_{0.48}As$ heterostructure, *Phys. Rev. Lett.*, 78 (7), 1335–1338.

[43] Zhong, Z., Tóth, A., and Held, K., 2013, Theory of spin-orbit coupling at LaAlO₃/SrTiO₃ interfaces and SrTiO₃ surfaces, *Phys. Rev. B*, 87 (16), 161102.

[44] Jang, C.W., Lee, W.J., Kim, J.K., Park, S.M., Kim, S., and Choi, S.H., 2022, Growth of two-dimensional Janus MoSSe by a single in situ process without initial or follow-up treatments, *NPG Asia Mater.*, 14 (1), 15.

[45] Qin, Y., Sayyad, M., Montblanch, A.R.P., Feuer, M.S.G., Dey, D., Blei, M., Sailus, R., Kara, D.M., Shen, Y., Yang, S., Botana, A.S., Atature, M., and Tongay, S., 2022, Reaching the excitonic limit in 2D Janus monolayers by *in situ* deterministic growth, *Adv.*

Mater., 34 (6), 2106222.

[46] Lin, Y.C., Liu, C., Yu, Y., Zarkadoula, E., Yoon, M., Puretzky, A.A., Liang, L., Kong, X., Gu, Y., Strasser, A., Meyer, H.M., Lorenz, M., Chisholm, M.F., Ivanov, I.N., Rouleau, C.M., Duscher, G., Xiao, K., and Geohegan, D.B., 2020, Low energy implantation into transition-metal dichalcogenide monolayers to form Janus structures, *ACS Nano*, 14 (4), 3896–3906.

[47] Volobuev, V.V., Mandal, P.S., Galicka, M., Caha, O., Sánchez-Barriga, J., Di Sante, D., Varykhalov, A., Khiar, A., Picozzi, S., Bauer, G., Kacman, P., Buczko, R., Rader, O., and Springholz, G., 2017, Giant Rashba splitting in $Pb_{1-x}Sn_xTe$ (111) topological crystalline insulator films controlled by bi doping in the bulk, *Adv. Mater.*, 29 (3), 1604185.